Na3V2(PO4)3-Supported Electrospun Carbon Nanofiber Nonwoven Fabric as Self-Standing Na-Ion Cell Cathode

ARTICLE

$Na_3V_2(PO_4)_3$–supported Electrospun Carbon Nanofiber Nonwoven Fabric as Self-Standing Na-ion Cell Cathode

G. Meligrana,*[a] S. Ferrari,[b] L. Lucherini,[c,d] J. Celè,[c,d] F. Colò,[a] J. Brugger,[d] C. Ricciardi,[c] R. Ruffo,[e] and C. Gerbaldi*[a]

[a] Dr. G. Meligrana, Dr. F. Colò, Prof. Dr. C. Gerbaldi
Group for Applied Materials and Electrochemistry (GAME Lab), Department of Applied Science and Technology (DISAT), Politecnico di Torino
Corso Duca degli Abruzzi 24, 10129, Torino, Italy
E-mail: giuseppina.meligrana@polito.it; claudio.gerbaldi@polito.it
[b] Dr. S. Ferrari
Department of Pharmacy, University of Chieti–Pescara "G. d'Annunzio"
Via dei Vestini 31, 66100, Chieti, Italy
[c] Mr. L. Lucherini, Mr. J. Celè, Prof. Dr. C. Ricciardi
Department of Applied Science and Technology (DISAT), Politecnico di Torino
Corso Duca degli Abruzzi 24, 10129, Torino, Italy
[d] Prof. Dr. J. Brugger
Microsystems Laboratory, École Polytechnique Fédérale de Lausanne - EPFL, 1015, Lausanne, Switzerland
[e] Prof. Dr. R. Ruffo
Department of Materials Science, Università di Milano-Bicocca
Via Roberto Cozzi 55, 20125, Milano, Italy

Supporting information for this article is given via a link at the end of the document.

Abstract: Sodium-ion technology is a reliable alternative to lithium-ion for large-scale energy storage because of the abundance of sodium sources and low cost. In this work we report about a simple fabrication of self-standing electrodes based on electrospun carbon nanofiber (CNF) loaded with $Na_3V_2(PO_4)_3$ with NASICON framework, which is a promising cathode material that has shown good electrochemical performance when its electrical conductivity is enhanced by a conductive medium. The proposed method is simple, low cost, potentially scalable to fabricate and load cathode support with active materials. The electrochemical tests confirmed the stable cycling performances and the high C-rate capability of the NVP-CNFs composites, with hundreds of cycles without major degradation of performances. Our work demonstrates that stable, self-supported, long-term performing NIB electrodes, ready to use without addition of any performance enhancer, can be obtained by using fast and cost-efficient procedures suitable to be scaled-up at an industrial level.

Introduction

Due to their high energy density and low weight, lithium-ion batteries (LIB) are used as energy storage devices in portable electronics and in electric mobility for e-bikes, electric cars, electric wheelchairs and modern hybrid vehicles. [1,2] The current Li-ion technology, based on Li^+ ion insertion/intercalation materials as anodes and cathodes, is well established. During the past years the energy density, cycle stability and safety of LIBs were improved in small evolutionary steps.[3,4] Although all the potential benefits that have been achieved using Li-ion technology, there are further studies that have explored the relationship between the availability of lithium resources and the likely future EV demand. Most have concluded that in the most optimistic EV markets the demand could not be covered by lithium availability.[5,6] Depletion of lithium availability and an increase in costs production create a necessity to explore alternatives to LIBs to solve the increasing demand for energy storage. There are few potential technologies yet to be developed that can overcome all the technical challenges of the Li-ion technology, among them electrochemistries based on magnesium, zinc, aluminium and sodium have gained interest [7,8].

Sodium-ion battery (Na-ion, NIB) is a promising alternative to LIB thanks to the abundance, the wide distribution, and the low cost of sodium and related raw materials.[9] Lately, active materials for positive and negative electrodes in SIBs have been the subject of much research and tremendous effort in developing cells showing high electrochemical performance. On the cathode side, the most investigated and promising active materials can be grouped into two families: layered metal oxides (LMOs) and polyanionic materials (phosphates, fluoro-phosphate, silicates, etc.)[10,12]. LMOs like $NaMnO_2$ or $NaFe_{0.5}Mn_{0.5}O_2$ show specific capacity up to 200 mAh g^{-1} and operating potential $\geq$ 3 V. The most remarkable feature is the low cost, abundance and environmental compatibility of precursors. Yet, they are highly sensitive to moisture and are reported to suffer from poor cycle life due to lattice deformation during intercalation/deintercalation. Among polyanion systems, Na ion super ionic conductor (NASICON) materials, like $Na_3V_2(PO_4)_3$, $Na_3Ti_2(PO_4)_3$ and $NaV(PO_4)F$, are characterized by high ionic conductivity (> 1 mS cm^{-1}), structural stability, specific capacity up to 180 mAh g^{-1} and voltages up to 3.4 V[13]. As a drawback, the very low electronic conductivity forces the use of conductive fillers or conductive electrode supports.[13, 14]

Carbon nanofibers (CNF) have been widely used in preparation of electrodes, mainly as conductive fillers,[15,16] anodic active materials[17,18] and conductive supports for cathodic active materials[19-21] due to their high electronic conductivity and mechanical properties. In fact, one dimensional (1D) nanofibers possess a unique structure that provides an enhanced surface-to-volume ratio, short transport length for ionic transport and efficient electron transport along the longitudinal direction. They can be produced via CVD techniques or standard polymeric manufacturing processes, such as spinning and electrospinning, starting from a carbon precursor solution.[22]

CNF may yield to self-standing conductive supports thus lowering the cost and the weight of batteries avoiding the use of metallic current collectors. Electrospinning is a versatile, easily scalable,

efficient and low-cost technique that has been broadly used recently to produce CNF with diameter ranging from 1 µm to 100 nm.[23,24] Frequently used polymers yielding high quality CNF are polyacrilonitrile (PAN), polyimide (PI), polyvinylidene fluoride (PVdF) and polyvinyl alcohol (PVA). PAN is frequently used to produce CNF with high carbon yield. After spinning, PAN fibers are first thermally stabilized in air between 200/300 °C and then pyrolyzed in inert atmosphere at temperature between 800/1500 °C to remove non-carbon atoms.

The high electrical conductivity (up to 1000 S cm^{-1}) and the porous interconnected structure of electrospun non-woven CNF are features that well match the requirements of an ideal battery electrode, offering low internal resistance and allowing electrolyte diffusion for the complete usage of the active material. Active materials suffering from low electronic conductivity and limited cycle life when used in slurry-based electrodes are reported to achieve better performances in terms of higher C rate, enhanced long-term cycling ability and higher Coulombic efficiency if combined with proper conductive supports. [16,19-21,25] Carbon-supported $Na_3V_2(PO_4)_3$/C has been the center of much research and interesting synthesis procedures and electrochemical results have been recently published.[26-28] Different carbon sources were also considered such as carbon nanospheres, carbon nanotubes and graphite nanosheets.[29] Electrospinning was employed to get NVP/C nanofibers, for example by the co-spinning method obtaining CNFs embedding NVP.[30,31] All those works show remarkable cycling results of $Na_3V_2(PO_4)_3$/C nanocomposites by using traditionally made electrodes based on a classical metal current collector onto which a slurry was spread. To the best of our knowledge, very little has been published about laboratory made electrospun CNFs where NVP is successively loaded, proposing self-standing electrodes and developing a general method easy to scale-up and adaptable to different materials and cells.

This is actually the aim of the present work, where CNF mats of different thicknesses were produced by electrospinning and morphological/compositional characterization was performed. Stabilization and carbonization of the CNF mat are investigated in detail to prove the reproducibility of the method and find useful correlation between the process parameters and the CNF mat morphology. The cathodic active material $Na_3V_2(PO_4)_3$ (NVP), was chosen due to the remarkable increase in cycle life performance when used in a conductive porous support.[20] NVP is directly loaded into the CNF support by dip coating and through vacuum filtration system, two low-cost and readily scalable techniques, which leads to a self-supported cathode ready to use without, in principle, any current collector support and/or the addition of any conductivity enhancer, thus in turn resulting in higher energy density at cell level. Electrochemical tests on the self-supported NVP/CNF cathode are conducted at ambient temperature in a laboratory-scale Na metal cell setup, which provide high specific capacity upon prolonged cycling, confirming for the first time the highly promising characteristics of such a simple, low-cost, easily scalable electrode setup.

Results and Discussion

CNF nonwoven fabric support

The experimental set-up of the electrospinning system used for the preparation of the CNF mats is shown in Fig. 1a. A PAN polymeric solution was fed through the needle at a constant and controlled rate, forming a pendant droplet at the needle tip. Charges were induced on the droplet surface by the electric field. When charges repulsion overcame solution surface tension, a jet was formed, protruding from the needle tip towards the collector. Jet stretching and solvent evaporation resulted in the reduction of the fiber diameter.

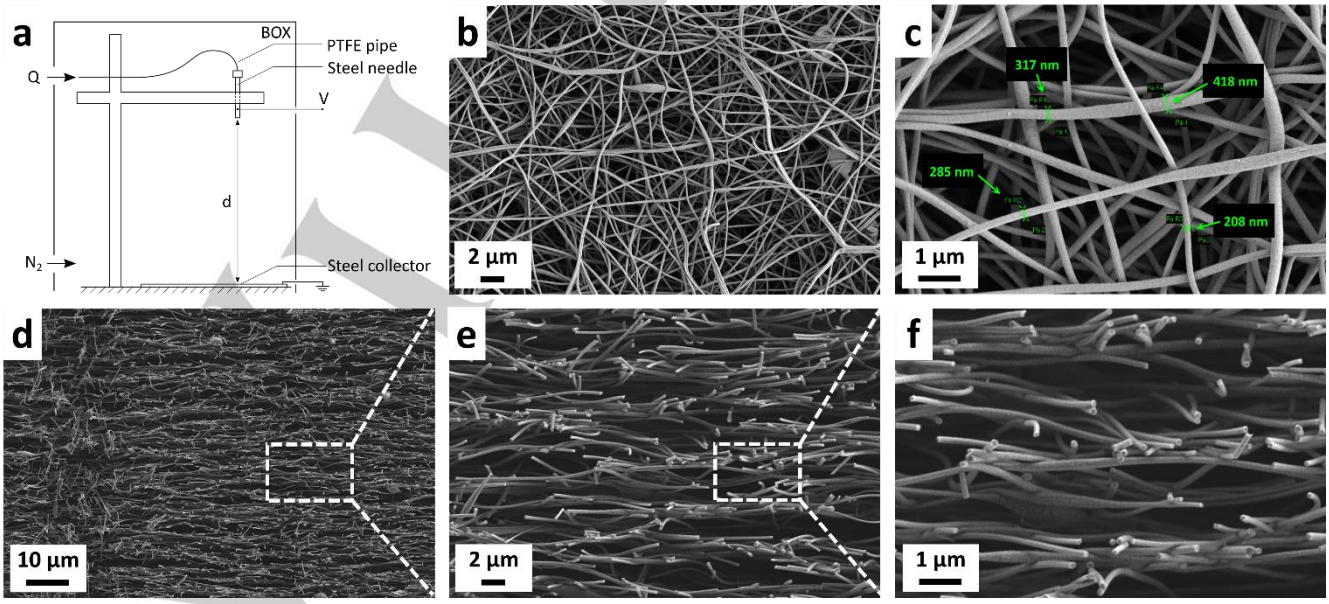

Figure 1. (a) Experimental electrospinning apparatus scheme; SEM images of (b) mat surface with randomly oriented fibres arranged in a non-woven structure and (c) example of spun fibers used for diameter measurement; (d, e, f) SEM images of a CNF cross section (carbonized fibers).

Figure 1b-c shows SEM images of the mat surface. The electrospun PAN mat covered a circular area of about 10 cm on the steel collector during the spinning process. After being peeled off, the mat was soft, bendable and easy to cut (see Fig. SI-1 in Supplementary Materials). The PAN fibers were distributed randomly on the surface and formed a non-woven texture with pores in the micron range determined by inter-fibers spacing and superposition. The estimated average diameter was 320(80) nm, similarly to values reported previously for the same PAN/DMAc solution and comparable set-up.[32]

The electrospinning technique provided a certain degree of flexibility to tune some nanofibers characteristics, such as the diameter of the fibres and other features related to the entire mat, *viz.* thickness. A thick mat can host more active material particles therefore increasing the cell energy, provided that the electrolyte diffusion is not hindered in a thicker electrode. Since mat thickness is a crucial parameter for an electrode support, experiments were performed in order to optimize it and investigate the relationship between the rate and volume of spun solution and the mat thickness. Thickness grew rapidly up to 500 µL of spun solution, then linearly up to 1 mL (see Fig. SI-2) and eventually slowed down for further volume increase (see Fig. SI-3, no major morphological differences are visible along the mat section). So far, few studies have been conducted on mat thickness growth[33] and the most recent works report CNF electrode support with thickness ranging only from 40 to 150 µm,[34,35] without any reference to the effect on cell performances. SEM images of a mat cross section (Figure 1d-f) revealed a structure formed by the stacking of several sheets composed of randomly oriented fibers. Cavities were formed where fibres sheets had no contact between each other so that interconnected pores were homogenously distributed along the section. Thin (50 µm) and thick mats (1 mm) were characterised by this same morphology that was retained also after the stabilization and carbonization steps. This investigation was also useful to assess the mechanical properties of mats of different thickness. The thicker the mat, the more brittle it resulted so that mats of thickness higher than about 70-80 µm were too soft to be cut without causing compressive stress and were not further tested for their electrochemical properties.

The stabilization was performed with a slow ramp of temperature first at 100, then at 200 °C and eventually at 260 °C. During this step the PAN reshapes its carbon structure in a more stable form thanks to a well-known intramolecular cyclization process of nitrile groups and an intermolecular cross-linking which stabilizes the polymer network; this is crucial for the mechanical properties of the fibers. In order to assess the optimal temperature and time for the stabilization, different conditions were initially chosen, and the stabilized PAN mats were studied by FTIR.

In Figure 2a, the evolution of the absorbance spectrum recorded at 260 °C after different times of stabilization is shown. The as prepared PAN mat is characterized by peaks at 2937, 2242 and 1452 cm^{-1}, assigned to C–H, C≡N and CH_2, respectively.[17,36] A strong peak was detected at 1629 cm^{-1} and assigned to the C=O of DMAc, meaning that traces of the solvent were still present in the as prepared mat and then fully removed during the stabilization step. The transformation of PAN is completed after 2 h of thermal treatment at 260 °C and was confirmed from the lowering of the intensity of the signature peaks and the appearance of strong new spectral features at 1581 cm^{-1} (C–C and C–N) 1363 cm^{-1} (C–N). The FTIR spectra of the CNF stabilized for 2 h at increasing temperature from 260 to 300 °C demonstrated no remarkable differences (Figure 2b). At lower temperature the stabilization was clearly incomplete and for these reasons the temperature for the stabilization was set at 260 °C. Incomplete stabilization led to a destructive effect on the fibers with partial melting of the PAN during the carbonization at high temperature as assessed on a sample stabilized at 200 °C and then carbonized (see Fig.SI-4).

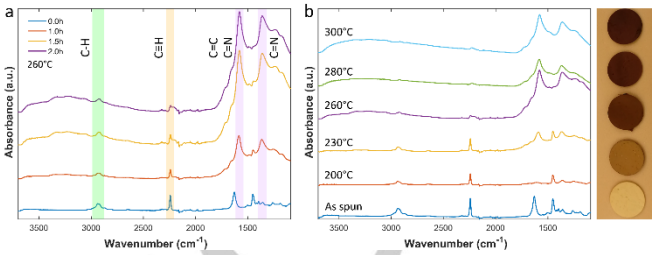

Figure 2. FTIR spectra of fibers stabilized at 260 °C for 1, 1:5 and 2 h. Spectrum of as spun fibers reported as 0:00 h. Relevant peaks for PAN and PAN stabilization are highlighted. b) FTIR spectra of fibers stabilized for 2 h at 200, 230, 260, 280 and 300 °C, respectively. On the right-hand side, colour variation of samples stabilized at 200, 230, 260, 280 and 300 °C (bottom to top), respectively.

The thermal annealing step at 900 °C in reducing atmosphere yielded the final conductive supporting carbon matrix. A typical CNF sample cut in disk is shown in Figure 3a together with the SEM image of its cross section (Figure 3b). The carbonized mats presented good mechanical stability and were easy to handle and punch with a 12 mm hand puncher. The Raman spectra of the CNF after stabilization and after carbonization are shown in Figure 3c. The typical D and G bands of carbon[37-39] were clearly visible for both the samples. The presence of an intense D band was expected due to the entirely amorphous phase of PAN in spun fibers whereas the G band arises for the emerging graphitic-like structure after stabilization.

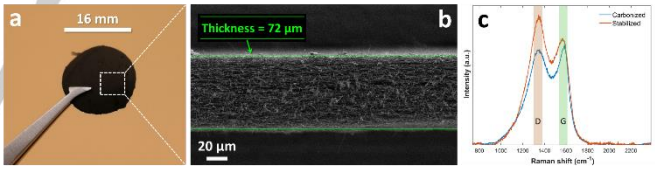

Figure 3. a) CNF disk and b) SEM image showing its cross section; c) Raman spectra of stabilized and carbonized fibers.

After carbonization there was a decreasing of the I_D/I_G ratio from 2.76 to 1.85, which suggests a partial reordering in polycrystalline domains of the original amorphous phase. This partial graphitic structure could favour the electrical conductivity of the fibers thus providing an optimal conducting support for the electrochemical reactions during the cell functioning. The measured transversal and longitudinal conductivity were 13(2) mS cm^{-1} and 423(4) mS cm^{-1}, respectively. The tenfold lower value of σ_t compared to σ_l was probably caused by the reduced contact among the fiber sheets along the transversal cross section of the mat, resulting in a higher impedance path. Longitudinal conductivity could instead be favoured by the high interconnection of fibers along the stacked planes.

NVP/CNF electrode characterisation

The NVP solution was used to prepare CNFs/NVP by dip-coating similarly to what previously reported by Yu et al.[19] where commercial CNFs were impregnated with a precursor solution

and, then, thermally treated to obtain the NASICON-type electrodes. The SEM images and EDX analysis of a representative NVP/CNF sample are shown in Figure 4a-c. The images and analysis revealed a not perfectly homogeneous distribution of the NVP nanoparticles on the fiber since the active material was found in higher concentration on one side of the CNF mat.

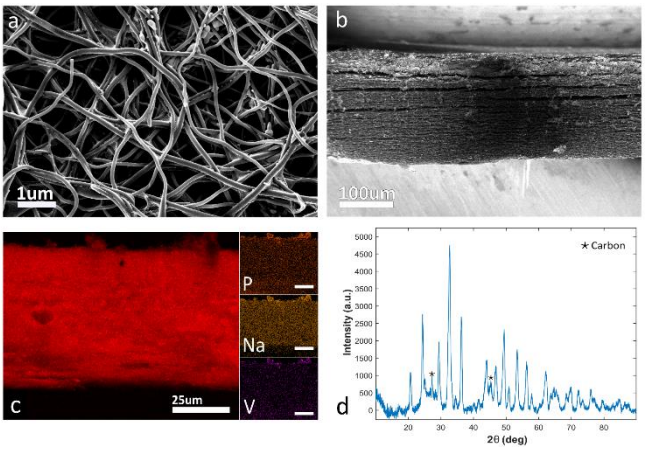

Figure 4. SEM images of the NVP/CNF surface (a) and cross section (b) prepared by dip coating; EDX analysis of the cross-section (c) and XRD pattern of NVP/CNF annealed at 800 °C for 8 h (d).

First, the EDX analysis confirmed the chemical composition and the homogeneous carbon distribution along the cross section. Then, it revealed that vanadium and phosphorous were present only in traces as an effect of the loading method. This phenomenon was probably due to the orientation of the carbon support during the drying step since some differences were observed in horizontally or vertically dried samples. Anyway, it was possible to establish on thicker samples that the active material particles can cover an area, which is 100 μm in thickness, so that it was decided to proceed with the electrochemical characterization of 70 μm thick samples.

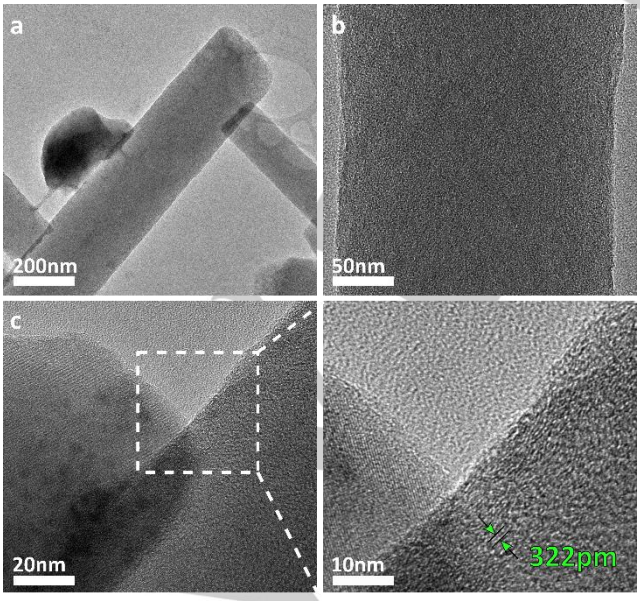

Figure 5. TEM images of NVP/CNF: a) CNF with NVP particle, b) CNF core and c) close-up on CNF surface at lower (left) and higher (right) magnification, showing polycrystalline order of small graphite domains.

The XRD pattern of an NVP/CNF sample thermally treated in Ar atmosphere at 800 °C for 8 h is shown in Figure 4d. It showed the peaks associated with the rhombohedral lattice of NVP (as detailed in Figure SI-5) together with peaks of carbon at 27° and 45° 2θ degrees, respectively, as previously reported also by other authors.[20] This sample was specifically prepared to confirm that the NVP precursor paste, showing only amorphous peaks at the XRD analysis, could effectively be annealed after loading to get crystalline NVP particles on the carbon nanofibers. A sample treated at the same temperature for 2 h did not show any crystalline phase in the XRD pattern. TEM was also used to investigate the crystallinity, fiber morphology of the NVP/CNF samples, and the NVP distribution on the carbon support. NVP particles were observed along the carbon nanofibers (Figure 5a) with an amorphous core (Figure 5b) coexisting with small polycrystalline regions (Figure 5c and close-up) for the presence of graphitic domains, thus confirming the Raman results.

Some tests were performed to assess the electrochemical activity of the NVP/CNF sample as cathode for Na-ion cells. NVP has been recently investigated because of its interesting electrochemical behaviour and theoretical capacity (117 mAh g^{-1}). Anyway, limited research has been carried out on NVP/CNF composites [14,15,19,31] that might be an appropriate strategy to overcome the poor electronic conductivity of this NASICON-type material that makes the theoretical capacity hardly achievable. The cyclic voltammetry results are shown in Figure 6.

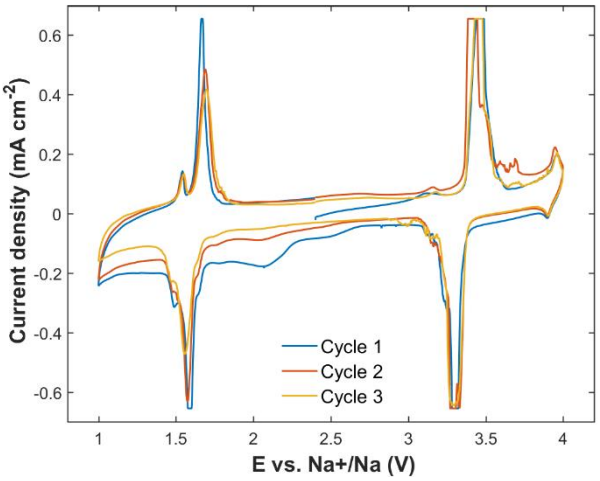

Figure 6. Cyclic voltammetry (CV) at 0.1 mV s^{-1} of the NVP/CNF cathode in the 1-4 V vs. Na^+/Na potential range.

A classical three-electrode cell with Na metal as counter electrode and the reference electrodes was used for this test. The active material loading (2 mg cm^{-2}) of the self-standing electrodes tested in Na half-cells was obtained by dip-coating. The theoretical capacity of such cells corresponded to 220 μAh cm^{-2}. Well defined, sharp redox peaks were detected both in oxidation and reduction due to the V^{3+}/ V^{4+} redox couple corresponding to the intercalation and deintercalation of Na^+ ions in the NVP crystal structure. Two reaction sites are related to those peaks and specifically the crystalline site M_2 (18e) (that is Na_2) is linked to the oxidation and reduction peaks detected in the CV plot at 3.46 and 3.30 V vs. Na^+/Na, respectively.[40] The separation between those peaks corresponds just to 55 mV, a very small value showing the good kinetic behaviour of the fiber supported electrode. A peak fitting was also carried out to get some more information about the

capacity of the material; by integrating the area of the peak at 3.46 V, a total capacity of 265 μAh cm^{-2} was obtained. The cell was discharged up to 1 V in order to explore the second electrochemically active region at low voltage. Sharp redox peaks were observed at about 1.60 V in good agreement with previous studies.[39] This reaction potential was attributed to the V^{3+}/V^{2+} redox couple, associated to a storage capacity of about 50 mAh g^{-1} for which the NVP properties as anode were also evaluated. Other small peaks that can be seen in the CV plot could originate from some structural reorganization related to the change of ion occupations, since various possibilities for the occupation of the interstitial sites have been proposed from both experimental and computational studies.[40,42]

The galvanostatic cycling test gave results in line with the CV peak fitting for the first cycle as can be seen from the plot in Figure 7a. After 70 cycles, the capacity was stable around 200 μAh cm^{-2} with an efficiency of 95 % (Figure 7b) which is lower than what was often reported for other NVP-based electrodes. This might be ascribed to the inherent characteristics of the carbon support, which resulted only partially graphitized after the annealing step; moreover, it is noteworthy that the electrodes did not include any conductive additive as normally found in literature, which could help in improving the round-trip efficiency.

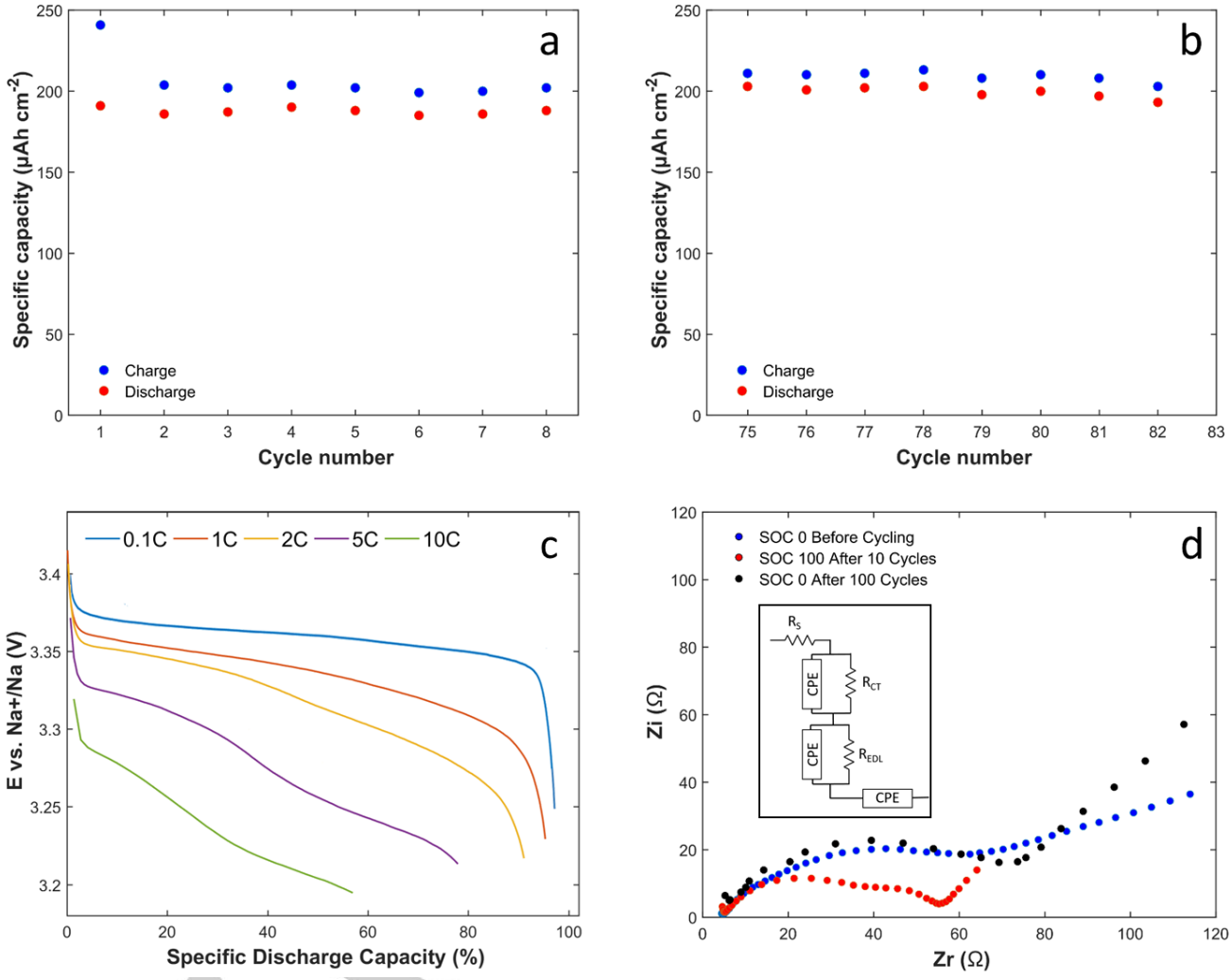

Figure 7. Electrochemical characteristics of the NVP/CNF-based lab-scale Na metal cell: a) and b) prolonged galvanostatic cycling at different cycles extracted from the same test at ambient temperature and fixed 1.5C rate, voltage range was 2.8-3.5V vs Na^+/Na; c) potential vs. discharge specific capacity profiles at different C rates and d) EIS spectra at different state of charge recorded during the 1.5C rate test.

The discharge profiles at different C-rates from 0.1 to 10C are shown in Figure 7c. Before each discharge, the cell was charged at 0.1C. The differences among the curves are evident in the 3.20 to 3.50 V voltage region and are related to three contributions, namely ohmic potential (IR) drop, activation polarization and concentration polarization. EIS was carried out at different SOCs (state of charge). The equivalent circuit used to explain the spectra (inset in Figure 7d) is R_S ($R_{EDL}CPE_{EDL}$) ($R_{CT}CPE_{DL}$) CPE_W where R_S is the electrolyte resistance, ($R_{EDL}CPE_{EDL}$) is a parallel between the resistance and the capacitance associated to the passivation layer, ($R_{CT}CPE_{DL}$) is a parallel between the electrical resistance associated with charge transfer processes and the double layer capacitance, finally CPE_W is associated with diffusion phenomena. The first spectrum recorded at SOC0, had similar shape compared to the one at the 100th cycle approximately after two weeks of cycling. An obvious difference

is in the low frequency diffusional tail associated to CPE_W, which is related to a different diffusion process in the cycled cell compared with the fresh one since the equilibrium condition of the fresh cell is not governed by the insertion reaction. Degradation of the electrolyte and continuous changes in the SEI layer could be responsible for a decreasing of the diffusion coefficient, which is inversely proportional to the slope on the Nyquist plot. The totally charged cell showed a completely different EIS spectrum, as expected. Two different depressed semicircles could be identified which are explained according to previously developed models [43-45]. The SOC100 measurement was taken when the charge was stopped and after some time for system equilibration. The potential dropped naturally from 3.5 to 3.37 V vs. Na^+/Na and the EIS spectrum was recorded. As reported previously,[45] the R_{EDL} shows a dependence on the potential with a marked difference between fresh and cycled cells. The additional medium frequency arc, which is not seen for the fresh cell, is ascribed to the charge transfer process. R_{CT} is obtained fitting the data (see Figure SI-6) and is quite similar for the fresh cell and the cycled for ten cycles (about 36 Ω), instead it almost doubled (61 Ω) after 100 cycles. This marked difference in R_{CT} after the galvanostatic cycling can be attributed to structural rearrangements in the material and to an increasing range of disorder in the active material particles that underwent continuous volume changes during cycling. The behaviour of CNFs should also be considered, including the contact interface around particles. R_{CT} was relatively low over the course of 100 cycles which could suggest a good conductive network. However, further experiments would be necessary to confirm this initial interpretation in which possible artefacts due to the cell configuration might lead to erroneous conclusions. It is still to clarify whether the reaction starts from the outer or from the inner part of the electrode since the CNFs are quite resistive (10^{-2} S cm^{-1}) compared with typical values for diffusion of about 10^4 S cm^{-1}. The cell was disassembled after the cycling and the cathode analysed with SEM to get some further information on the morphology of the SEI layer (Figure SI-7). Many pores of the CNF appeared clogged due to the presence of a very thick SEI layer, which led to a higher capacitance when the cell was fully discharged. However, an amount of pores was still open, which accounts for the good cycling behaviour at high C rate and the observed stability in the electrochemical performances.

A second method for producing NVP/CNF in the form of self-standing cathodes was developed, consisting in filtering the NVP precursor solution directly on the carbon nanofibers mat by means of Buchner filtration. To the best of the authors' knowledge, so far, no works have been presented which have studied this process for NIB. This preliminary exploration was conducted to test faster processes possibly offering a better control on the active material loading and profile deposition. This is a very simple and frequently used technique in chemical labs that might enable the preparation of electrodes in a fast and cheap way. The thickness of the mat used for this method was 50 µm, in order to favour a homogeneous distribution of the NVP precursor among the nanofibers. In the SEM images recorded after filtration (see Figure SI-8) the NVP particles are clearly visible. The active material distribution profile had a peak at the surface of the mat but the NVP particles were observed also in the bulk. This result suggests that filtration could be an effective way to better control the loading with respect to dip coating. Currently, preliminary results have showed that the NVP crystallization step needs more investigation. This procedure required a different annealing process in order to optimize the CNF mat, which was not ideal for obtaining crystalline NVP. The XRD diffractogram recorded on the annealed sample did not show the typical peaks related to the crystalline NVP phase (Figure SI-9). In any case, some electrochemical test and mainly the CV results indicated the presence of likely amorphous NVP with the oxidation peak recorded at 3.40 V vs. Na^+/Na. The easiness in controlling the active material particle loading motivates further research in this direction.

Conclusion

NVP/CNF composite electrodes were prepared starting from electrospun carbon nanofibers. Electrospun CNF were initially produced and stabilization and carbonization of the CNF mat were investigated in detail to optimize the process parameters and the CNF mat morphology.

NVP is a promising NASICON type cathode material for Na-ion technology. To fully take advantage of the energy capacity of this material and concurrently reach an improved design of the whole cell, we suggest an alternative approach, which is favourable in improving the transport properties of the electrode. NVP/CNF self-standing electrodes were prepared by dip-coating or Büchner filtration which were considered as straightforward loading methods. The electrochemical tests confirmed the good cycling performances and the high C-rate capability of the NVP-CNFs composite: more than 200 cycles have been performed, without major degradation of performances.

We proposed a simple, low cost, potentially scalable process to fabricate and load cathode support with active materials. The general concept behind the CNF support and loading procedure is not linked to any specific material and any other active compound than NVP, appropriately prepared, can possibly be processed in the same way. Overall, the results here presented demonstrate that stable, self-supported, long-term performing electrodes, ready to use without addition of any performance enhancer, are obtained by using fast and low cost procedures suitable to be scaled-up at an industrial level, because of energy and time saving preparation, thus enlightening that these kinds of materials are interesting candidates for future applications in next generation 3D-lithium-based microbatteries.

Experimental Section

Nanofiber mat synthesis

The nanofiber membranes were prepared through an electrospinning procedure. Polyacrylonitrile (PAN, *M*w = 150,000, Aldrich) was dispersed in *N,N*-dimethylacetamide (DMAc, Aldrich) and magnetic stirred for 36 h at 60 °C. The concentration of the solution was fixed at 8 wt% as reported by Lee et al.[32]

The polymeric solution was fed through a blunt-tipped syringe needle (Ø = 0.8 mm, stainless steel) by means of an infusion syringe pump (Harvard Apparatus PHD Ultra), at constant flow rate of 1.5 mL h^{-1}, while applying a 14 kV DC voltage. The syringe was connected to the needle with PTFE connectors and PTFE pipe. The distance between the needle and collector (grounded, static stainless-steel collector covered with Al foil) was 15 cm. The apparatus was placed inside a plexiglass box to control environmental parameters. Humidity level was regulated using nitrogen flow inside the box and monitored with a Sensirion humidity sensor. A digital camera was

used to monitor the spinning process. The relative humidity and the environmental temperature were 35 % and 23 °C, respectively.

The electrospun mats were stabilized in air, in a Thermo Scientific Heraeus oven by a multi-step process including three temperature ramps and dwell time: 100 °C for 30 min, then 200 °C for 30 min, and lastly 260 °C for 120 min. Carbonization was performed at 900 °C for 2 h under Ar flow at a heating rate of 5 °C min^{-1}.[25]

Cathode active material $Na_3V_2(PO_4)_3$ (NVP) synthesis

The NVP cathode material was synthesised through coprecipitation.[20] A 0.25 M solution of NH_4VO_3 (ACS reagent 99.0 %, Aldrich) in deionized water was added with oxalic acid (99 %, Aldrich) in 0.75 M concentration in order to turn the oxidation state of vanadium to 4+. After 12 h of magnetic stirring at 50 °C, sodium acetate (ACS reagent 99 %, Aldrich) and ammonium phosphate (ACS reagent 99 %, Honeywell) solutions in stoichiometric amount were added slowly to the previous dark blue solution. After 6 h of stirring at 80 °C, the liquid precursor was evaporated, and a green paste deposited. The paste was completely dried in oven at 120 °C for 2 h and kept in a drier until further use.

Self-standing NVP/CNF cathodes preparation

Two procedures, namely dip coating and Buchner filtration, were used to load the active material particles on the produced CNF mat.

For the dip coating, small pieces of about 3 cm^2 of the carbonized fibres were immersed in 4 mL of the NVP precursor solution described just above and left to stand for 12 h. After soaking, the fibres were dried in an air oven (Thermo Scientific Heraeus) at 120 °C for 2 h. Before assembling the electrochemical cell, the NVP/CNF sample was annealed in Ar atmosphere for 8 h at 800 °C with heating rate 5 °C min^{-1} to obtain the crystalline NVP phase.

In the second loading procedure, the CNF mat was used as filtering paper in a Buchner filtration system. NVP precursor solution was dropped on the CNF mat and vacuum filtered. Vacuum was removed after few minutes and the CNF mat was dried in an air oven. The sample was annealed for 2 h at 800 °C with heating rate 5 °C min^{-1} in Ar atmosphere to crystallize the NVP.

Materials characterization

X-ray powder diffraction (XRD) was carried out by using a PANalytical Empyrean diffractometer in the 10-90° 2theta range (0.02° step size and step scan 2 s).

Scanning Electron Microscopy (SEM) images and EDX maps were collected by using a Zeiss Gemini 300 SEM on samples coated with 5nm thick sputtered carbon. FEI Talos TEM was used for TEM imaging and EDX on NVP/CNF powder samples. For TEM analysis, NVP/CNF powder was dispersed in ethanol and dropped on copper support grids.

The FTIR spectra were acquired by a Nicolet 6700 spectrometer in ATR mode. Scans were acquired from 600 to 4000 cm^{-1}. Baseline removal and peaks match were performed with Nicolet software. Spectra used for comparison on samples treated at different stabilization temperatures were scaled by a common factor for better highlighting relevant peaks.

Raman spectra of CNF mat before and after carbonization were acquired with a Renishaw inVia microscope in the 700-2400 cm^{-1} range with excitation wavelength of 532 nm.

The conductivity of CNF through and along the mat plane (σ_t; σ_l, transversal and longitudinal, respectively) was evaluated. A two probes measurement set-up (see Supplementary material) was used to measure the transversal and longitudinal resistance (R_t; R_l). Contacts to the CNF were made with copper tape (resistance < 0.01 Ω) mounted on glass slide. A second glass slide was used to apply uniform pressure on top of the CNF. Current was swept from -1 to 1 mA with a step of 0.10 mA (Keithley 2400 Source Meter; Keithley 2000 Multimeter for voltage measurement). Data were acquired with a LabView software already available in the laboratory. Mean value and standard deviation were evaluated over five samples (MATLAB).

Cell assembly and electrochemical measurements

Three-electrode Swagelok type cells were assembled in an Ar-filled glove box (MBraun UNILab, H_2O and O_2 < 0.1 ppm). The NVP/CNF self-standing electrodes were tested as cathodes in lab-scale Na cells with Na metal used as counter and reference electrodes. Whatman glass fibre membrane was used as separator impregnated with an electrolyte comprising 1 M $NaClO_4$ in 50:50 weight mixture of ethylene carbonate and poly(ethylene carbonate). The NVP active material content in the electrode was about 2.0 mg cm^{-2}.

All electrochemical measurements were performed with a Gamry Reference 600 at ambient laboratory temperature. Cyclic voltammetry was performed in the range from 1.6 to 4 V vs. Na^+/Na at a 0.10 mV s^{-1} scan rate. Galvanostatic cycling was carried out at different current rates from 0.1 to 10C in the 2.8-3.5 V vs. Na^+/Na range.

Electrochemical Impedance Spectroscopy (EIS) was performed in the frequency range from 1 Hz to 100 kHz with a sinusoidal signal of 10 mV.

Acknowledgements

Financial support from the Italian Government, Ministry of Education, Universities and Research – MIUR (PRIN N° 2017MCEEY4 funding) is gratefully acknowledged.

The ENABLES project (http://www.enables-project.eu/) has received funding from the European Union's Horizon 2020 research and innovation program, under Grant Agreement no. 730957.

Keywords: Sodium ion battery • Carbon nanofiber • sodium ion vanadium phosphate • NASICON compound • electrospinning

References

[1] P.G. Bruce, B. Scrosati, J.-M. Tarascon, *Angew. Chem. Int. Ed.* **2008**, *47*, 2930-2946.
[2] M. Li, J. Lu, Z. Chen, K. Amine, *Adv. Mater.* **2018**, *30*, 1800561
[3] B. Scrosati, *Solid State Electrochem.* **2011**, *15*, 1623-1630.
[4] A. Manthiram, X. Yu, S. Wang, *Nat. Rev. Mater.* **2017**, *2*, 16103
[5] A. Mauger, C. M. Julien, *Ionics* **2017**, *23*, 1933-1947.
[6] M. Bini, D. Capsoni, S. Ferrari, E. Quartarone, P. Mustarelli in *Rechargeable lithium batteries: from fundamentals to applications (*Eds.: by A. A. Franco) Woodhead Publishing Limited, **2015**, 1-17.
[7] A. Ponrouch, M. Rosa Palacín, *Phil. Trans. R. Soc. A* **2019**, *377*, 20180297
[8] J.-M. Tarascon, *Phil. Trans. R. Soc. A* **2010**, *368*, 3227-3241.
[9] C. Vaalma, D. Buchholz, M. Weil, S. Passerini, *Nat. Rev. Mater.* **2018**, 3, 18013.
[10] C. Delmas, *Adv. En. Mat.* **2018**, *8*, 1-9.
[11] S. Chen, C. Wu, L. Shen, C. Zhu, Y. Huang, K. Xi, J. Maier, Y. Yu, *Adv. Mater.* **2017**, *29*, 1700431.
[12] Q. Wang, M. Zhang, C. Zhou, Y. Chen, *J. Phys. Chem C* **2018**, *122*, 16649-16654.
[13] X. Xiang, Q. Lu, M. Han, J. Chen, *Chem. Comm.* **2016**, *52*, 3653-3656.
[14] J. Yang, D.-W. Han, M. R. Jo, K. S., Y.-I. Kim, S.-L. Chou, H.-K. Liu, Y.-M. Kang, *J. Mater. Chem. A* **2015**, 3, 1005-1009.
[15] H. Li, Y. Bai, F. Wu, Y. Li, C. Wu, *J. Power Sources* **2015**, *273*, 784-792.

[16] B. Zhang, Y. Yu, Z.-L. Xu, S. Abouali, M. Akbari, Y.-B. He, F. Kang, J.-K. Kim, *Adv. Energy Mater.* **2014**, *4*, 1301448.
[17] Y. Liu, F. Wang, L. Z. Fan, *Nano Res.* **2018**, 11, 4026-4037.
[18] T. Jin, Y. Liu, Y. Li, K. Cao, X. Wang, L. Jiao, *Adv. En. Mater.* **2017**, *7*, 1700087.
[19] S. Yu, Z. Liu, H. Tempel, H. Kungl, R.-A. Eichel, *J. Mater. Chem. A* **2018**, *6*, 18304-18317.
[20] Y. Peng, R. Tan, J. Ma, Q. Li, T. Wang, X. Duan, *J. Mater. Chem. A* **2019**, *7*, 14681-14688.
[21] B. Zhang, F. Kang, J. M. Tarascon, J. K. Kim, *Prog. Mater. Sci.* **2016**, *76*, 319-380.
[22] J.-W. Jung, C.-L. Lee, S. Yu, I.-D. Kim, *J. Mater. Chem. A* **2016**, *4*, 703-750.
[23] L. Li, S. Peng, J.K. Y. Lee, D. Ji, M. Srinivasan, S. Ramakrishna, *Nano Energy* **2017**, *39,* 111-139.
[24] L. Wu, Y. Hao, S. Shi, X. Zhang, H. Li, Y. Su, L. Yang, S. Zhong, *Frontiers Chem.* **2018**, *6*, 1-9.
[25] Q. Duan, B. Wang, J. Wang, H. Wang, Y. Lu, *J. Power Sources* **2010**, *195*, 8189-8193.
[26] X. Cao, A. Pan, B. Yin, G. Fang, Y. Wang, X. Kong, T. Zhu, J. Zhou, G. Cao, S. Liang, *Nano Energy* **2019**, *60*, 312-323.
[27] W. Yang, W. He, X. Zhang, G. Yang, J. Ma, Y. Wang, C. Wang, *ChemElectroChem* **2019**, *6*, 2020-2028.
[28] X. Wan, K. Liu, P. Lei, W. Zheng, X. Xiang, M. Sun, *ChemElectroChem* **2018**, *5*, 2630-2635.
[29] S. Li, Y. Dong, L. Xu, X. Xu, L. He, L. Mai, *Adv. Mater.* **2014**, *26*, 3545-3553.
[30] L. Wu, S. Shi, X. Zhang, Y. Yang, J. Liu, S. Tang, S. Zhong, *Electrochim. Acta* **2018**, *274*, 233-241.
[31] J. Liu, K. Tang, K. Song, P. A. van Aken, Y. Yu, J. Maier, *Nanoscale* **2014**, *6*, 5081-5086.
[32] J. Lee, Y. H. Jeong, D. W. Cho, *Macromol. Mater. Eng.* **2014**, *299,* 1052-1061.
[33] K. Liu, P. Lei, X. Wan, W. Zheng, X. Xiang, *J. Coll. Interf. Sci.* **2018,** *532*, 426-432.
[34] R. Chen, Y. Hu, Z. Shen, P. Pan, X. He, K. Wu, X. Zhang, Z. Cheng. *J. Mater. Chem. A* **2017**, *5*, 12914-12921.
[35] M. M. Coleman, R. J. Petcavich, *J. Polym. Sci. Polym. Phys. Ed.* **1978**, *16*, 821-832.
[36] M.S.A. Rahaman, A.F. Ismail, A. Mustafa, *Polym. Degr. Stab.* **2007**, *92*, 1421-1432.
[37] C. Kim, S.-H. Park, J.-I. Cho, D.-Y. Lee, T.-J. Park, W.-J. Lee, K.-S. Yang, *J. Raman Spectrosc.,* **2004***, 35,* 928-933.
[38] P. Suresh Kumar, R. Sahay, V. Aravindan, J. Sundaramurthy, W. Chui Ling, V. Thavasi, S. G. Mhaisalkar, S. Madhavi, S. Ramakrishna, *J. Phys. D: Appl. Phys.* **2012**, *45*, 265302.
[39] M.J. Song, T. Kim, Y.B. Kim, M.W. Shin, *Electrochim. Acta* **2015**, *182*, 289-296.
[40] Z.L. Jian, C. C. Yuan, W. Z. Han, X. Lu, L. Gu, X. K. Xi, Y. S. Hu, H. Li, W. Chen, D. F. Chen, Y. Ikuhara, L. Q. Chen *Adv. Funct. Mater.* **2014**, *24*, 4265-4272.
[41] K. Saravanan, C. W. Mason, A. Rudola, K. H. Wong, P. Balaya, *Adv. Energy Mat.* **2013,** *3*, 444-450.
[42] W. Song, X. Ji, Z. Wu, Y. Zhu, Y. Yang, J. Chen, M. Jing, F. Li, C. E. Banks, *J. Mater. Chem. A* **2014**, *2*, 5358-5362.
[43] D. Andre, M. Meiler, K. Steiner, C. Wimmer, T. Soczka-Guth, D.U. Sauer, *J. Power Sources* **2011,** 196, 5334-5341.
[44] M. Grossi, B. Riccio, *J. Sensors and Sensor Systems* **2017**, *6*, 303-325.
[45] M.D. Levi, K. Gamolsky, D. Aurbach, U. Heider, R. Oesten, *Electrochim. Acta* **2000,** *45*, 1781-1789.

Entry for the Table of Contents

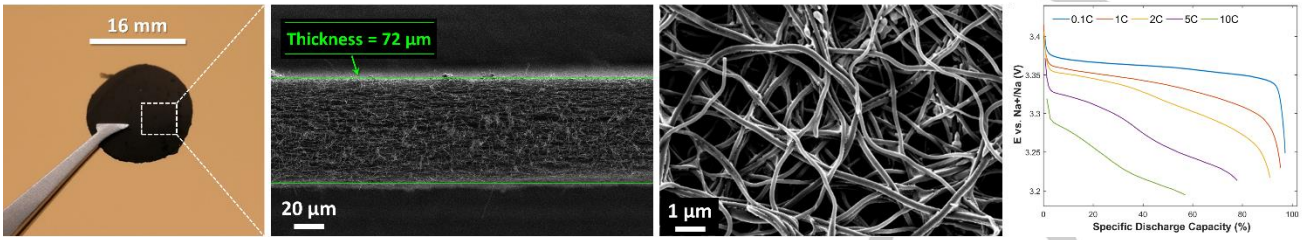

Self-standing, composite Na-ion battery cathodes comprising NASICON-type $Na_3V_2(PO_4)_3$ loaded onto electrospun carbon nanofibers are prepared by simple, low cost, potentially scalable procedure, which is favourable in improving the transport properties of the active material without addition of any performance enhancer, resulting in enhanced cycling performances chiefly at high C-rate, without major degradation of performances.

https://www.facebook.com/GAMELabPoliTO, https://twitter.com/PoliTOnews